FERMILAB-CONF-06-145-AD

ANALYSIS OF EMITTANCE GROWTH IN THE FERMILAB BOOSTER*

X. Huang, SLAC, Stanford, CA 94309, S.Y. Lee, U. of Indiana, Bloomington, IN 47405,
K.Y. Ng, Fermilab, Batavia, IL 60510, USA

Abstract

Multi-particle simulations are performed to study emittance growth in the Fermilab Booster. Analysis shows that the source of vertical emittance growth comes mostly from random errors in skew quadrupoles in the presence of a strong transverse space-charge force. [1] Random errors in dipole rolls and the Montague resonance do contribute but to lesser extent. The effect of random errors in the quadrupoles is small because the betatron envelope tunes are reasonably far away from the half-integer stopband.

IPM MEASUREMENTS

The transverse rms beam radii $\sigma_{x,z}$ of the Fermilab Booster have been measured [2] using the ionization beam profile monitor (IPM) at the location where the betatron functions and dispersion are $\beta_{x,z} \approx 6.5/20.5$ m and $D \approx 1.8$ m. The IPM has a gate of $\sim 1\,\mu$s allowing ~ 52 bunches to pass through. The vertical rms emittance is $\epsilon_z = \sigma_z^2/\beta_z$, which is plotted for the whole ramp cycle in Fig. 1 at 4- and 12-turn injections. Also shown are the normalized rms emittances ϵ_z^n, which starts from $\sim 2\,\pi$mm-mr almost independent of intensity (there is no painting), but increases rapidly within the first 4000 revolutions (region A) at higher beam intensity. It then grows almost linearly between 4000 to 1700 revolutions (region B), after which extraction takes place. The aim of this article is to understand the growth mechanism.

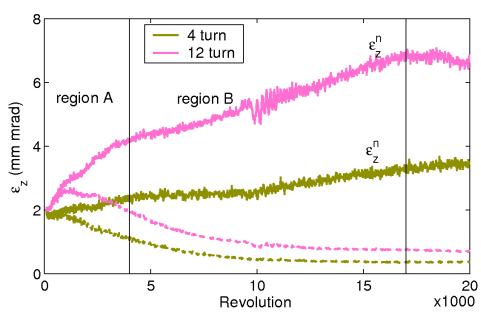

Figure 1: (Color) Rms normalized vertical emittances ϵ_z^n. The unnormalized emittances ϵ_z are shown in dashes.

The emittance growth per revolution in both regions can be fitted rather well up to 12-turn injection according to

$$\frac{d\epsilon_z^n}{dn} = b_1 + b_2 K_{\rm sc},$$

where $K_{\rm sc}$ is the space-charge perveance, with only three parameters: $b_1 \approx 0.8 \times 10^{-4}\,\pi$mm mr/rev, $b_2 \approx 0.8 \times 10^4$ πmm mr/rev, and $\epsilon_z^n(0) \approx 1.8\,\pi$mm mr. Obviously, the space-charge term dominates in region A. In region B, however, the linear term dominates, since $K_{\rm sc}$ dwindles down rapidly as the beam energy increases. The reason of the linear growth of $\sim 1\,\pi$mm mr/10^4 rev is not clear. Residual gas scattering at the 100-nTorr vacuum and intrabeam scattering contribute, respectively, only $d\epsilon_z^n/dn \approx 2.4{\times}10^{-4}\,\pi$mm mr/$10^4$ rev and $\leq 3{\times}10^{-5}\,\pi$mm mr/$10^4$ rev.

The horizontal beam size σ_x receives contribution from the betatron emittance ϵ_x and the dispersion D according to $\sigma_x^2 = \beta_x\epsilon_x + D^2\sigma_\delta^2$. These two contributions have very different dependency on the relativistic parameters γ and β, as well as the rf voltage and synchronous phase. As a result, the two contributions can be separated so that the emittance ϵ_x and momentum spread σ_δ along the ramp cycle can be extracted. The calculated results fit the bunch length and momentum spread of various intensities measured separately at the wall-gap monitor, as demonstrated in Fig. 2 with a single set of parameters assuming the longitudinal bunch area of 0.08 eVs. We do not find explosive ϵ_x^n blow-up as ϵ_z^n in region A. Instead the growth rate of ϵ_x^n in the whole cycle is roughly the same as ϵ_z^n in region B.

Post-transition, there is bunch length oscillation coming from phase-space mismatch as the space-charge force changes sign. From the oscillation amplitude, the longitudinal bunch area can be deduced. The non-oscillatory part can be separated again into the emittance and dispersion components as before.

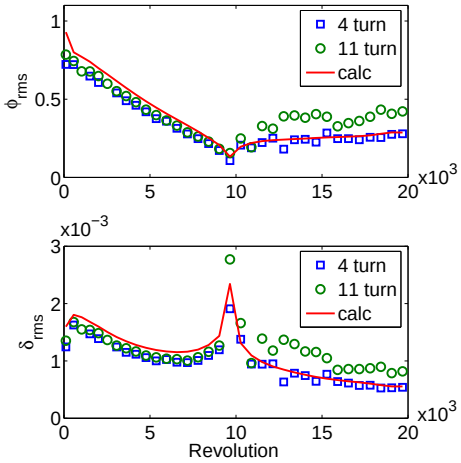

Figure 2: (Color) Bunch length and momentum spread calculated from IPM results (solid) agree well with data obtained from a resistive-wall monitor up to 10-turn injection below 9200 revolution.

MODELING AND SIMULATIONS

Multi-particle simulations are performed hoping that the IPM results could be modeled.

1. Since the Booster is composed of 24 combined-function FODO cells, transport matrices $M_{D\to F}$ and $M_{F\to D}$ are employed for each half cell, using measured tunes and Twiss parameters along the ramp cycle.

2. Systematic sextupoles, random dipoles, quadrupole, and skew quadrupole errors are introduced as kicks:

$$x'' + K_x(s)x = b_0(s) + b_1(s)x + a_1(s)z - \tfrac{1}{2}b_2(s)(x^2 - z^2),$$
$$z'' + K_z(s)z = -a_0(s) - b_1(s)z + a_1(s)x + b_2(s)xz.$$

* Work supported by NSF PHY-0552389, DOE DE-FG02-92ER40747, and DOE DE-AC02-76CH03000.

3. Dipole errors are designed to mimic injection closed orbit-errors, which are usually damped in $N_{\rm dip} \sim 3000$ rev. Thus the error amplitude damping factors $A_{a0,b0}(n) = A_{a0,b0}(0)e^{-n/N_{\rm dip}}$ are included in the simulations.
4. Random quadrupole errors are introduced satisfying $\oint \beta_x(s)b_1(s)ds = 0$ and $\oint \beta_z(s)b_1(s)ds = 0$ so that the tunes are not perturbed. Quadrupole errors are to account for phase-space mismatch, which is usually damped in $N_{\rm quad} \sim 4000$ rev. Thus the error amplitude damping factors $A_{a1,b1}(n) = A_{a1,b1}(0)e^{-n/N_{\rm quad}}$ are included.
5. Body sextupoles are introduced as thin-lens kicks at the end of each half cell with the measured strengths $\int b_2 ds = -0.0173$ and $-0.263\,\mathrm{m}^{-2}$, respectively, at the F and D quadrupoles. Chromaticity sextupoles have also been included, but their effects on emittances are small, since wake fields driving collective instabilities are not considered here.
6. Bi-Gaussian distributed beam is employed and we assume the distribution to maintain bi-Gaussian even when the beam is perturbed. The space-charge potential is

$$V(x,z) = \frac{Nr_0}{\beta^2\gamma^3}\int_0^\infty \frac{-1+\exp\{-\frac{x^2}{2\sigma_x^2+t}-\frac{z^2}{2\sigma_z^2+t}\}}{\sqrt{(2\sigma_x^2+t)(2\sigma_z^2+t)}}dt$$
$$\approx -\frac{Nr_0}{\beta^2\gamma^3}\left\{\left[\frac{x^2}{\sigma_x(\sigma_x+\sigma_z)}+\frac{z^2}{\sigma_z(\sigma_x+\sigma_z)}\right]-\right.$$
$$\left.-\frac{1}{4\sigma_x^2(\sigma_x+\sigma_z)^2}\left(\frac{2+r}{3}x^4+\frac{2}{r}x^2z^2+\frac{1+2r}{3r^3}z^4\right)+\cdots\right\},$$

where $r = \sigma_z/\sigma_x$. Thus the space-charge kicks are

$$\Delta x' = -\frac{\partial V}{\partial x}\ell \approx \frac{2Nr_0\ell}{\beta^2\gamma^3\sigma_x(\sigma_x+\sigma_z)}x\,e^{-(x^2+z^2)/(\sigma_x+\sigma_z)^2},$$
$$\Delta z' = -\frac{\partial V}{\partial z}\ell \approx \frac{2Nr_0\ell}{\beta^2\gamma^3\sigma_z(\sigma_x+\sigma_z)}z\,e^{-(x^2+z^2)/(\sigma_x+\sigma_z)^2},$$

where ℓ is half-cell length and N is the linear particle density in the beam. Exponentiated forms are used to allow for negligible tune shifts for large-amplitude particles.
7. The rf and synchronous-phase tables for the actual ramp are used. In addition, the measured bunch length is employed to compute bunching factor and momentum spread. The measured 95% longitudinal bunch area is 0.08 eVs.
8. Post-transition momentum-spread oscillation due to space-charge mismatch is put in by hand. For $n > n_t = 9600$, it is

$$\sigma_\delta(n) = \sigma_{\delta 0}B_f(n)\left\{1+\left(G_\delta-1\right)\left[1-e^{-\alpha_\delta(n-n_t)}\right]\right\}\times$$
$$\times\left[1+A_\delta e^{-\alpha_\delta(n-n_t)}\sin 2\pi f(n-n_t)\right], \qquad (1)$$

with initial rms momentum spread $\sigma_{\delta 0} \approx 3.0\times 10^{-4}$, growth factor $G_\delta = 2.0$, oscillation amplitude $A_\delta = 0.5$, frequency $f = \frac{1}{150}\,\mathrm{rev}^{-1}$, and decoherence factor $\alpha_\delta = \frac{1}{15\times 150}$.

SIMULATION RESULTS

Half-Integer Stopbands

Stopband widths are intentionally made larger at harmonic 13 and small at 12 by special choice of random seed of quadrupole errors. The result of 12-turn injection with quadrupole error 40×10^{-4} m^{-1}, about 1.3% of the main quadrupole field (~ 10 times too large), is shown in Fig. 3, where we see large emittance increase when the bare tunes are near the half-integer stopband. Only the linear part of space charge is included. The vertical bare tune is fixed at $\nu_z = 6.95$ while the horizontal bare tune varies from $2\nu_x = 12$ to 14. Space charge usually self-adjusts when the beam is sufficiently near the stopband. Particles redistribute and the bunch may become hollow so that the emittance growth is reduced.

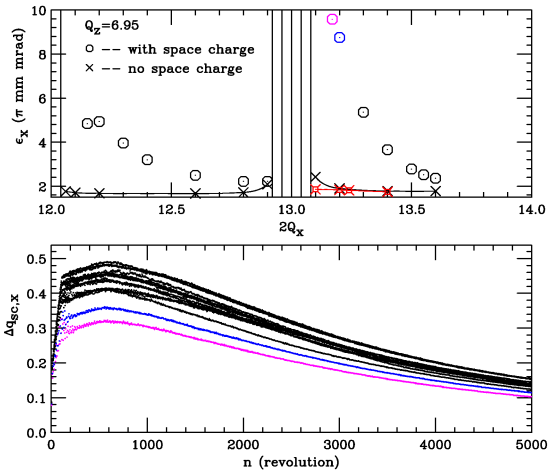

Figure 3: (Color) Top: Plot showing large emittance growth when the horizontal tune approaches and is inside the half-integer stopband. Bottom: Horizontal space-charge tune shift corresponding to various points in the top plot.

Montague Resonance

The $2\nu_x - 2\nu_z = 0$ Montague resonance is driven by nonlinear space charge. To study the resonance, we perform simulation at 12-turn injection by turning off all linear random errors. Although Montague resonance can cause emittance exchange, its effect on emittance growth is small.

Skew Quadrupole Errors

Skew quadrupole field can be induced by quadrupole roll and vertical closed orbit deviation in sextupole. With a 1-cm amplitude of vertical closed orbit error inside the sextupole field, the feed-down skew quadrupole amplitude is estimated to be 35×10^{-4} m^{-1} (focal length 300 m). To avoid mixing with the effects of Montague resonance, we try at 12-turn injection to vary the strength of skew quadrupole errors as 0, 3.5×10^{-4}, 14×10^{-4}, and 35×10^{-4} m^{-1}, but keeping identical random seed. The bare vertical tune is kept fixed at $\nu_z = 6.85$ while the bare horizontal tune is varied from $\nu_x = 6$ to 7.

Without skew quadrupole field, we see in Fig. 4 just small Montague resonance when $\nu_x = \nu_z$ and $\epsilon_x \approx \epsilon_y$. When ν_x approaches an integer, ϵ_x^n diverges. The effects are not much different at skew quadrupole strength 3.5×10^{-4} m^{-1} As the strength increases to 0.0014 and 0.0035 m^{-1}, both linear difference and sum resonances become important with $\epsilon_{x,z}$ increase. Beam loss occurs even when the tunes are far away from sum resonance. Near the sum resonance, particles redistribute themselves and the bunch becomes hollow in both transverse phase spaces. Figure 5 show the increase of the sum resonance stopband

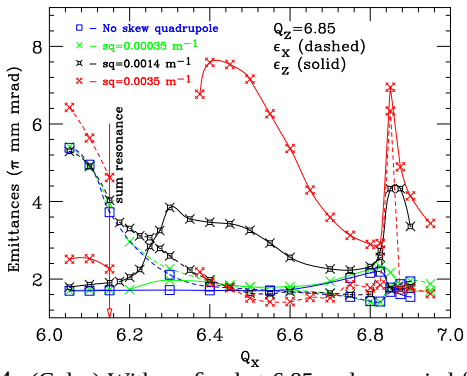

Figure 4: (Color) With ν_z fixed at 6.85 and ν_x varied from 6.0 to 7.0, four different strengths of skew quadrupole field are studied. The emittances increase sharply and beam loss occurs at the difference resonance and near the sum resonance at high skew quadrupole field.

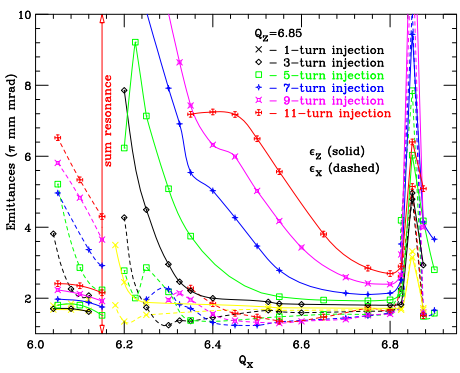

Figure 5: (Color) Sum stopband is found to increase with beam intensity with skew quadrupole component at 0.0035 m^{-1}.

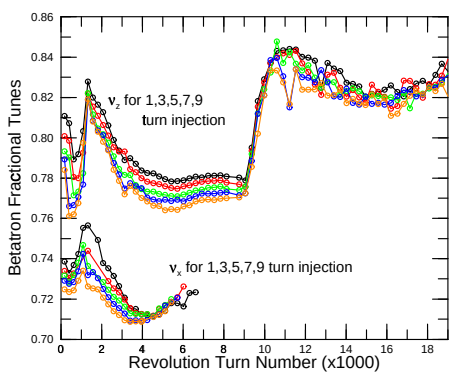

Figure 6: (Color) Betatron tunes measured using a vertical pinger on May 7, 2005. They satisfy the best setting of $\nu_z - \nu_x \approx 0.1$ for all beam intensities in this analysis.

as the beam intensity increases from 1- to 11-turn injection. To minimize emittance growth, one should therefore choose $\nu_z - \nu_x \approx 0.1$, which is actually the setting used in operation at the present, as demonstrated in Fig. 6 by the tunes measured recently using a vertical pinger. [2]

Dipole Errors

Dipole errors generate coherent beam oscillations. Nonlinearities convert coherent oscillations into emittance growth. Magnet rolls generate horizontal magnetic field, thus vertical dipole error will in general be larger than the horizontal. Reasonable dipole errors are 7.5×10^{-5} rad vertical and 2.0×10^{-5} rad horizontal. [3] This leads to a faster increase in ϵ_z^n than ϵ_x^n, as demonstrated in Fig. 7.

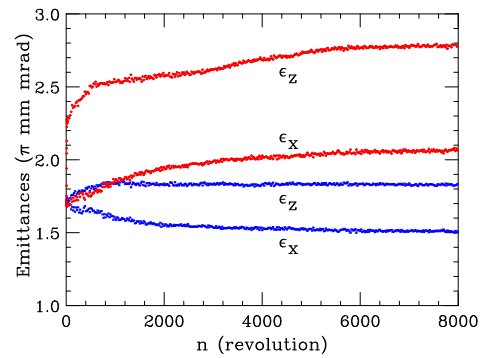

Figure 7: (Color) Since vertical dipole error is usually much larger than horizontal dipole error, we see a much larger growth in ϵ_z^n than ϵ_x^n (red) to be compared with the situation of no dipole errors (blue).

SUMMARY

Putting all considerations together, the simulated beam radii and the normalized emittances at an F-quadrupole are shown in Fig. 8, resembling what were measured. The conclusion is that the emittance increases at 12-turn injection arise from: skew quadrupole errors $\sim 50\%$, dipole errors $\sim 25\%$, and space charge $\sim 25\%$. The skew quadrupole errors broaden the sum-resonance stopband which enhances emittance growths as intensity increases. The simulated ϵ_z^n's at various-turn injection in region A also agree with measurement. The initial increases of $\epsilon_{x,z}^n$ come probably from phase-space mismatch in the presence of space charge and dipole errors. The mismatch magnitude is proportional to the space-charge perveance K_{sc}, which explains why we can fit ϵ_z^n with $d\epsilon_z^n/dn \sim K_{sc}$ for the first 4000 rev.

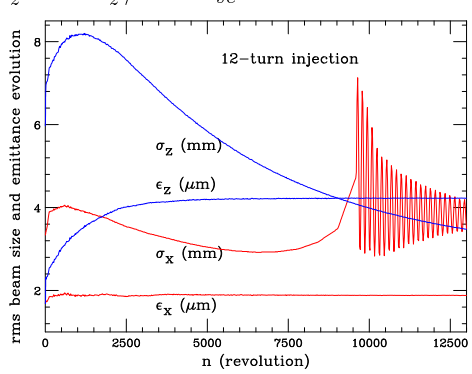

Figure 8: (Color) Simulated normalized emittances and beam sizes at an F-quad for a beam with 12-turn injection resemble what were measured.

REFERENCES

[1] X. Huang, S.Y. Lee, K.Y. Ng, and Y. Su, *Emittance Measurement and Modeling for the Fermilab Booster*, Phys. Rev. ST Accel. Beams **9**, 014202 (2006).

[2] X. Huang, *Beam Diagnosis and Lattice Modeling of the Fermilab Booster*, PhD thesis, Indiana University, 2005.

[3] X. Huang, S.Y. Lee, C.M. Ankenbrandt, and E. Prebys, *Fitting the Fully Coupled ORM for the Fermilab Booster*, PAC'05, Knoxville, TN, May 16-20, 2005.